ZYG-9, TAC-1 and ZYG-8 together ensure correct microtubule function throughout the cell cycle of *C. elegans* embryos

Jean-Michel Bellanger[1],*, J. Clayton Carter[2], Jennifer B. Phillips[2,‡], Coralie Canard[1], Bruce Bowerman[2] and Pierre Gönczy[1,§]

[1]Swiss Institute for Experimental Cancer Research (ISREC), Swiss Federal Institute of Technology (EPFL), School of Life Sciences, Lausanne, Switzerland
[2]Institute of Molecular Biology, University of Oregon, Eugene, OR 97403, USA

*Present address: CRBM-CNRS, 34293 Montpellier Cedex 5, France
‡Present address: Institute of Neuroscience, University of Oregon, Eugene, OR 97403, USA
§Author for correspondence (e-mail: Pierre.Gonczy@isrec.unil.ch)

Summary

The early *Caenorhabditis elegans* embryo is well suited for investigating microtubule-dependent cell division processes. In the one-cell stage, the XMAP215 homologue ZYG-9, associated with the TACC protein TAC-1, promotes microtubule growth during interphase and mitosis, whereas the doublecortin domain protein ZYG-8 is required for anaphase spindle positioning. How ZYG-9, TAC-1 and ZYG-8 together ensure correct microtubule-dependent processes throughout the cell cycle is not fully understood. Here, we identify new temperature-sensitive alleles of *zyg-9* and *tac-1*. Analysis of ZYG-9 and TAC-1 distribution in these mutants identifies amino acids important for centrosomal targeting and for stability of the two proteins. This analysis also reveals that TAC-1 is needed for correct ZYG-9 centrosomal enrichment. Moreover, we find that ZYG-9, but not TAC-1, is limiting for microtubule-dependent processes in one-cell-stage embryos. Using two of these alleles to rapidly inactivate ZYG-9–TAC-1 function, we establish that this complex is required for correct anaphase spindle positioning. Furthermore, we uncover that ZYG-9–TAC-1 and ZYG-8 function together during meiosis, interphase and mitosis. We also find that TAC-1 physically interacts with ZYG-8 through its doublecortin domain, and that in vivo TAC-1 and ZYG-8 are part of a complex that does not contain ZYG-9. Taken together, these findings indicate that ZYG-9–TAC-1 and ZYG-8 act in a partially redundant manner to ensure correct microtubule assembly throughout the cell cycle of early *C. elegans* embryos.

Supplementary material available online at
http://jcs.biologists.org/cgi/content/full/120/16/2963/DC1

C. elegans, TAC-1, ZYG-8, ZYG-9, Cell cycle, Microtubules

Introduction

Regulation of microtubule behavior is crucial for correct cell division. Microtubule dynamics is governed by the intrinsic properties of the polymer and microtubule-associated proteins (MAPs). Whereas much is known about the mechanisms by which MAPs influence microtubule dynamics in vitro, comparatively little is known about how they function in vivo.

The early embryo of *Caenorhabditis elegans* is an attractive model system to investigate microtubule-dependent processes within live cells, owing notably to the exquisite temporal and spatial resolution that can be achieved with time-lapse differential interference contrast (DIC) microscopy (reviewed in Oegema and Hyman, 2005). Distinct microtubule-dependent processes occur during the first cell cycle, including migration of the male and female pronuclei during interphase, as well as spindle assembly during mitosis. Importantly, forward genetic and functional genomic studies have led to the systematic identification of genes required for correct microtubule-dependent processes, including genes encoding MAPs.

Correct growth of microtubules in eukaryotic cells generally relies on a XMAP215-related MAP (reviewed in Kinoshita et al., 2002). Originally identified as a growth-promoting factor in *Xenopus* egg extracts (Gard and Kirschner, 1987), XMAP215 and related proteins are thought to favor polymerization of microtubules, although XMAP215 itself and its *S. cerevisiae* homologue Stu2p can also promote microtubule depolymerization (Shirasu-Hiza et al., 2003; van Breugel et al., 2003). In *C. elegans* embryos, the XMAP215 homologue ZYG-9 is present in the cytoplasm and enriched at centrosomes throughout the cell cycle (Matthews et al., 1998). Embryos depleted of ZYG-9 exhibit slower rates of microtubule growth and, consequently, have shorter astral microtubules (Srayko et al., 2005). As a result, several microtubule-dependent processes fail in the one-cell stage (Kemphues et al., 1986). For instance, male and female pronuclear migration are defective during interphase and, as a consequence, the spindle assembles in an aberrant position during mitosis. Thus, ZYG-9 is required for microtubule growth throughout the cell cycle but the consequences of inactivating it solely during mitosis have not been addressed.

In several organisms, XMAP215 family members associate with a protein of the transforming and acidic coiled-coil (TACC) family (reviewed in Gergely, 2002). In *Drosophila*, TACC is required for the efficient recruitment of the

XMAP215 protein Msps to centrosomes (Cullen and Ohkura, 2001; Lee et al., 2001). Similarly, TACC3 helps recruit the XMAP215 protein ch-TOG to spindle microtubules in human cells (Gergely et al., 2003). In *C. elegans*, the only TACC family member TAC-1 localizes in the cytoplasm and is enriched at centrosomes, like ZYG-9 (Bellanger and Gönczy, 2003; Le Bot et al., 2003; Srayko et al., 2003). Moreover, ZYG-9 and TAC-1 form a complex and stabilize each other in vivo: in either *zyg-9*(*RNAi*) or *tac-1*(*RNAi*) embryos, both ZYG-9 and TAC-1 protein levels are severely diminished (Bellanger and Gönczy, 2003). Therefore, in the absence of mutant alleles to analyze the contribution of each protein separately, it is not clear whether either ZYG-9 or TAC-1 is limiting for promoting microtubule growth in vivo.

Another MAP acting in the one-cell stage *C. elegans* embryo is ZYG-8, which harbors a doublecortin domain and a kinase domain (Gönczy et al., 2001). ZYG-8 is enriched at microtubule asters throughout the cell cycle and is present on the spindle during mitosis. The evolutionarily conserved doublecortin domain binds microtubules and promotes their stability or polymerization (reviewed in Horesh et al., 1999). In humans, the doublecortin gene DCX is mutated in patients with a neuronal migration disorder thought to result from defective microtubule-dependent processes (des Portes et al., 1998; Gleeson et al., 1998). Furthermore, the mammalian orthologue of ZYG-8, known as DCLK (doublecortin-like kinase), regulates spindle assembly and ensures the correct fate of cortical neural progenitors (Shu et al., 2006). In *C. elegans*, *zyg-8*-mutant embryos undergo a sequence of events comparable with that in the wild type during interphase. During mitosis, however, they exhibit a defect in anaphase spindle positioning that results in aberrant cell division (Gönczy et al., 2001). An analogous phenotype is observed after treatment of wild-type embryos with nocodazole during mitosis (Gönczy et al., 2001), indicating that ZYG-8 acts during that stage of the cell cycle to promote microtubule growth, a conclusion supported by measurements of growth rates in metaphase *zyg-8*(*RNAi*) embryos (Srayko et al., 2005). However, whether *zyg-8* also acts during interphase is not apparent from this analysis, nor that of null-mutant alleles (Gönczy et al., 2001). The absence of a requirement during interphase might reflect the fact that ZYG-8 acts strictly during mitosis. Alternatively, ZYG-8 might act throughout the cell cycle but become essential only during mitosis when the requirement for growth promoting factors may be particularly high.

Here, we report the identification of new *zyg-9* and *tac-1* alleles that allowed us to address several questions regarding the respective contribution of ZYG-9 and TAC-1 to microtubule-dependent processes in vivo. Moreover, we were able to achieve rapid conditional inactivation of the ZYG-9–TAC-1 complex and, thus, test its requirement specifically during mitosis. In addition, using synthetic gene inactivation, we demonstrate that ZYG-9–TAC-1 and ZYG-8 act in a partially redundant manner throughout the cell cycle of one-cell stage *C. elegans* embryos.

Results

Identification of new mutant alleles of *zyg-9* and *tac-1*
We identified eight conditional-recessive parental-effect embryonic-lethal mutant strains with phenotypes at the

Table 1. Embryonic lethality of new *zyg-9* and *tac-1* temperature-sensitive alleles

| Genotype	Lethality 15°C (in %)	Lethality 26°C (in %)
N2 (wild-type)	<1 (409)	<1 (548)
zyg-9(*or593*)	73 (265)	99 (167)
zyg-9(*or623*)	<1 (311)	100 (314)
zyg-9(*or628*)	42 (301)	100 (230)
zyg-9(*or634*)	<1 (321)	100 (277)
zyg-9(*or635*)	6 (286)	100 (341)
tac-1(*or369/402*)	50 (317)	97 (564)
tac-1(*or455*)	0 (326)	>99 (301)

Embryonic lethality conferred by animals of the indicated genotypes raised at the indicated temperatures. The number of embryos scored is given in parentheses.

restrictive temperature that are indistinguishable from those observed when *zyg-9* or *tac-1* is inactivated (Materials and Methods; Table 1). We genetically mapped the mutation in five mutant strains to the center of chromosome II, where *zyg-9* is located, and in three mutant strains to the right arm of chromosome II, where *tac-1* is located (Materials and Methods). The five strains of the first group fail to complement each other and *zyg-9*(*b244*), demonstrating that they correspond to *zyg-9*-mutant alleles. The three strains of the second group also fail to complement each other.

We conducted western blot analysis of embryonic extracts from each mutant strain to estimate the overall levels of TAC-1 or ZYG-9 protein (see supplementary material Fig. S1). These extracts were prepared from embryos at all developmental stages and, thus, might only partially reflect the impact of the mutations on TAC-1 and ZYG-9 in the early embryo. Therefore, we systematically examined the distribution of ZYG-9 and TAC-1 in early embryos by immunofluorescence analysis in the eight mutant strains at the restrictive temperature. Representative specimens are shown in Figs 1 and 2, which also report quantification of the cytoplasmic and centrosomal protein levels observed in each case. In addition, we performed sequence analysis of the eight mutant strains.

Analysis of *zyg-9* alleles
Sequencing of the *zyg-9* gene in the first complementation group revealed the following point mutations (Fig. 1A and supplementary material Fig. S2A): D189G in *zyg-9*(*or623*), G203E in *zyg-9*(*or628*), G488E in *zyg-9*(*or593*), I862K in *zyg-9*(*or635*) and E1317K in *zyg-9*(*or634*). The mutations in *zyg-9*(*or623*), *zyg-9*(*or628*), *zyg-9*(*or593*) and *zyg-9*(*or635*) lie in three so-called TOG domains that are found in all members of the XMAP215 family and are likely to mediate tubulin binding (supplementary material Fig. S2A) (Al-Bassam et al., 2007). TOG domains form paddle-like structures composed of six HEAT (huntingtin, elongation factor 3, PP2A regulatory subunit, TOR1) repeats (HR1 to HR6) (Al-Bassam et al., 2007). HEAT repeats form rod-like helical structures and mediate protein-protein interactions (Andrade and Bork, 1995), suggesting that these four *zyg-9* alleles encode proteins defective in binding tubulin and/or another partner protein. We found that centrosomal ZYG-9 is decreased in two of these alleles, *zyg-9*(*or628*) and *zyg-9*(*or593*), despite cytoplasmic levels being comparable to those of the wild type (Fig. 1F,1H).
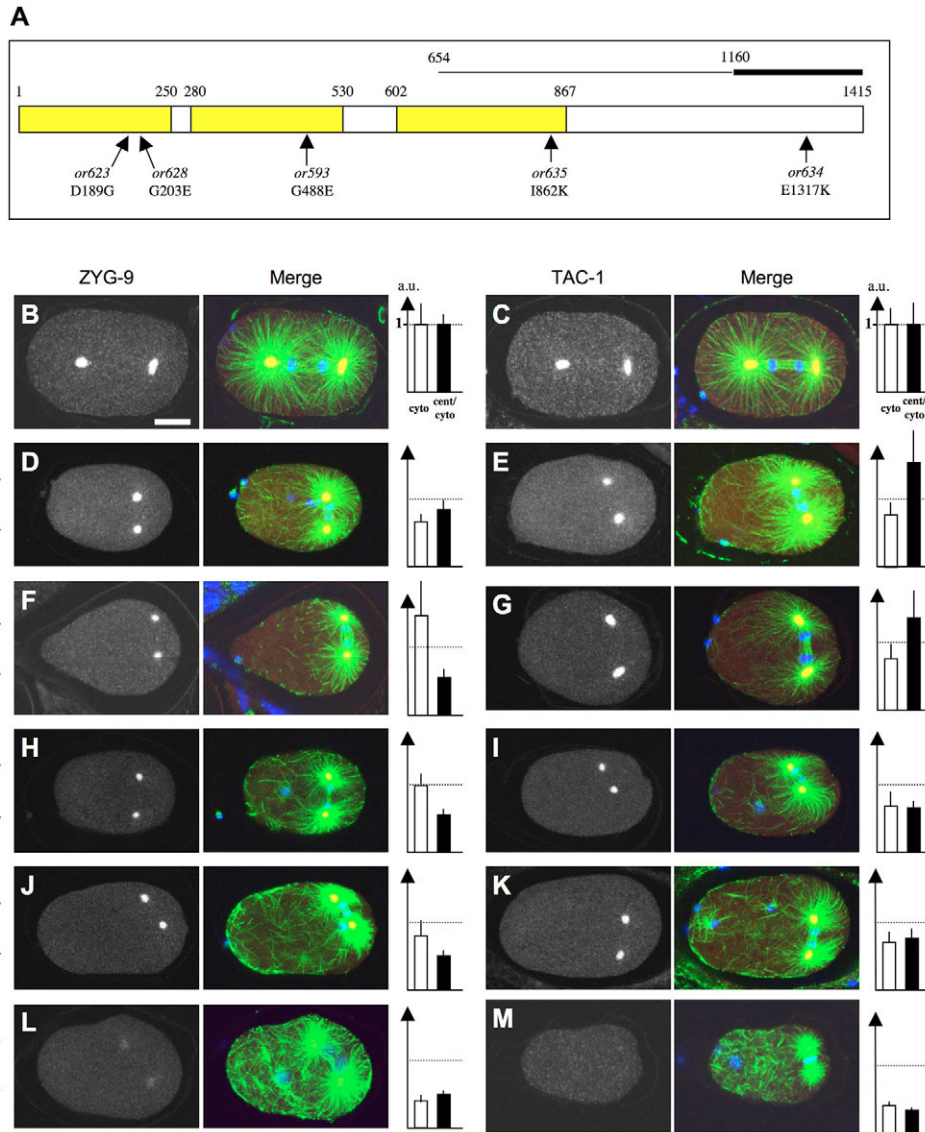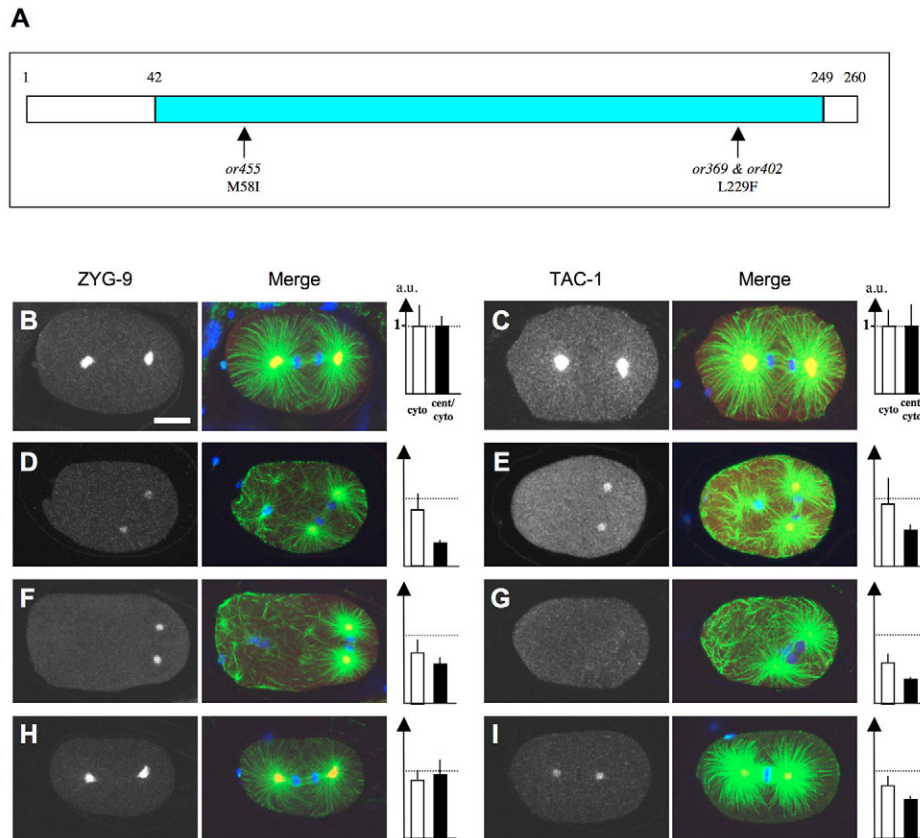
Fig. 1. Molecular lesions, TAC-1 and ZYG-9 distribution in five new *zyg-9* temperature-sensitive mutant alleles. (A) Schematic representation of ZYG-9 (1-1415) showing the position and nature of the mutations identified in the five new *zyg-9* alleles. Yellow boxes, TOG domains; line above the protein, TAC-1-binding region TBR (thick line, strong binding; thin line, weak binding) (Bellanger and Gönczy, 2003). (B-M) One-cell-stage embryos during mitosis in the wild-type (B,C) or *zyg-9* (D-M) temperature-sensitive mutant alleles shifted at 25°C for >12 hours and stained with antibodies against ZYG-9 (B,D,F,H,J,L) or TAC-1 (C,E,G,I,K,M) and α-tubulin. Left panels show ZYG-9 or TAC-1 staining alone, right panels the merge of ZYG-9 or TAC-1 (red), α-tubulin (green) and DNA (blue). The histograms on the right of each staining series represent the quantification of ZYG-9 and TAC-1 levels in the cytoplasm (white bars) and the ratio between the levels of ZYG-9 or TAC-1 at centrosomes and in the cytoplasm (black bars) (Materials and Methods). Values are given as the mean ± s.e.m.; a.u., arbitrary units relative to the wild-type values, which have been set to 1 (dashed lines). Numbers of embryos analyzed for TAC-1 and ZYG-9 were: wild type, 17 and 13; *zyg-9(or593)*, 10 and 9; *zyg-9(or623)*, 10 and 13; *zyg-9(or628)*, 10 and 8; *zyg-9(or634)*, 11 and 10; *zyg-9(or635)*, 10 and 10. Anterior is left, posterior is right; bar, 10 μm. Images in panels D, E and K are maximum-intensity projection of two ~1-μm-thick confocal sections; the remaining images are single 1-μm-thick confocal sections. We found also that the distribution of ZYG-9 and TAC-1 is comparable with that of the wild type in *zyg-9(or623)*, *zyg-9(or634)* and *zyg-9(or635)* embryos at 15°C (data not shown).

It is tempting to speculate that the alteration in the TOG domains 1 and 2 in these two alleles compromises interaction with a centrosomal anchor. Although the nature of such a putative TOG-domain-interacting centrosomal anchor remains to be determined, it is unlikely to be TAC-1 because a fragment of ZYG-9 lacking the two first TOG domains can still interact with TAC-1 (Bellanger and Gönczy, 2003).

The I862K mutation in *zyg-9(or635)* changes an amino acid that is invariant and located within a conserved stretch of amino-acids in all metazoan XMAP215 family members (see supplementary material Fig. S2A). We found that, in this allele, ZYG-9 is also significantly decreased at centrosomes and, to a lesser extent, in the cytoplasm (Fig. 1J). As I862 is also part of a weak TAC-1-binding region (TBR, Fig. 1A) (Bellanger and Gönczy, 2003), it is possible that the I862K mutation alters formation of the TAC-1–ZYG-9 complex. To test this

Fig. 2. Molecular lesions, TAC-1 and ZYG-9 distribution in three new *tac-1* temperature-sensitive mutant alleles. (A) Schematic representation of TAC-1 (1-260) showing the position and nature of the mutations identified in the three new *tac-1* alleles. Cyan box, TACC domain. (B-I) One-cell-stage embryos during mitosis in the wild-type (B,C) and *tac-1* temperature-sensitive mutant alleles shifted at 25°C for >12 hours (D-G) or maintained at 15°C (H,I). B,D,F,H: ZYG-9 and α-tubulin staining; C,E,G,I,: TAC-1 and α-tubulin staining. Left panels show ZYG-9 or TAC-1 staining alone, right panels the merge of ZYG-9 or TAC-1 (red), α-tubulin (green) and DNA (blue). The histograms on the right of each staining series represent the quantification of ZYG-9 and TAC-1 levels in the cytoplasm (white bars) and the ratio between the levels of ZYG-9 or TAC-1 at centrosomes and in the cytoplasm (black bars) (Materials and Methods). Values are given as the mean ± s.e.m.; a.u., arbitrary units relative to the wild-type values, which have been set to 1 (dashed lines). Numbers of embryos analyzed for TAC-1 and ZYG-9 were: wild type, 17 and 13; *tac-1(or369)* plus *tac-1(or402)*: 19 and 18; *tac-1(or455)*, 10 and 10; *tac-1(or455)* [15]: 11 and 14. Anterior is left, posterior is right; bars, =10 μm.

hypothesis, we performed an in vitro binding assay using the TBR of ZYG-9 I862K and GST-TAC-1. As shown in Fig. 3, we found that the I862K mutation causes a sizeable reduction in the ability of the TBR of ZYG-9 to bind TAC-1. Accordingly, we observed a slight reduction of TAC-1 levels in *zyg-9(or635)* early embryos (Fig. 1K), as anticipated if the interaction between TAC-1 and ZYG-9 is less efficient in vivo.

Although the E1317K mutation in *zyg-9(or634)* represents a drastic electrostatic change, this region of the protein is quite divergent among XMAP215 family members; an arginine occupies this position in vertebrates, demonstrating that a positively charged amino-acid can be accommodated at this site (see supplementary material Fig. S2A). Nonetheless, in *C. elegans*, this mutation results in a severe decrease of ZYG-9 levels, both at centrosomes and in the cytoplasm (Fig. 1L). E1317 is located within a domain that undergoes robust interaction with TAC-1 (Bellanger and Gönczy, 2003), raising the possibility that the E1317K mutation disrupts TAC-1 binding. Accordingly, we found that the E1317K mutation causes a significant reduction in the binding of the ZYG-9 TBR

to TAC-1 (Fig. 3). Compatible with this view, TAC-1 levels are also markedly decreased in *zyg-9(or634)* embryos, both at centrosomes and in the cytoplasm (Fig. 2M). Overall, the analysis of these newly identified *zyg-9* alleles uncovers new centrosomal targeting and protein-stabilizing functions for the ZYG-9 TOG domains, as well as for the two residues I862 and E1317 that are also crucial for efficient binding to TAC-1.

Analysis of *tac-1* alleles

Sequencing the *tac-1* gene in the second complementation group revealed the following point mutations (Fig. 2A and supplementary material Fig. S2B): L229F in both *tac-1(or369)* and *tac-1(or402)* (hence considered collectively as *tac-1(or369)* in the entire manuscript) and M58I in *tac-1(or455)*. These strains identify the first mutant alleles of *tac-1*. The residues mutated in these alleles are not invariant across evolution. Nevertheless, they are part of the TACC domain (Fig. 2A and supplementary material Fig. S2B), whose function is likely to be hampered by the mutations. We found that centrosomal TAC-1 is diminished approximately twofold

in *tac-1(or369)* embryos and approximately threefold in *tac-1(or455)* embryos compared with the wild type (Fig. 2E,G). By contrast, cytoplasmic TAC-1 levels in *tac-1(or369)* embryos are comparable to those in the wild type and slightly diminished in *tac-1(or455)* embryos (Fig. 2E,G). We addressed whether these two mutations impair the interaction between TAC-1 and ZYG-9. We found that, whereas the binding of GST-TAC-1 M58I to the ZYG-9 TBR is not impaired, that of GST-TAC-1 L229F is severely diminished compared with the wild type (Fig. 3). Overall, we conclude that the mutations M58I and L229F both alter the ability of TAC-1 to be targeted or retained at centrosomes. Furthermore, we conclude that, M58I has an additional, slightly deleterious effect on protein stability and L229 is crucial for ZYG-9 binding.

The new mutant alleles provide new insight into the function of ZYG-9–TAC-1

Inactivation of either ZYG-9 or TAC-1 using RNA interference (RNAi) compromises the entire ZYG-9–TAC-1 complex, a fact that has precluded an analysis of the relative contribution of each protein separately. For instance, it is not known whether each protein can be present at centrosomes without the other, nor whether either ZYG-9 or TAC-1 is limiting for microtubule-dependent processes in one-cell-stage embryos. We reasoned that an examination of ZYG-9 and TAC-1 distribution in a selection of our newly identified mutant alleles might shed light on these questions.

First, centrosomal TAC-1 is not reduced in *zyg-9(or628)* embryos, despite centrosomal ZYG-9 being approximately twofold lower than in the wild type (Fig. 1G,F). Therefore, centrosomal ZYG-9 is not limiting for the presence of TAC-1 at centrosomes. Second, despite being present at relatively normal levels in the cytoplasm, centrosomal ZYG-9 is severely diminished in *tac-1(or369)* embryos (Fig. 2D), in which centrosomal but not cytoplasmic TAC-1 is diminished (Fig. 2E). This indicates that centrosomal TAC-1 is limiting for ZYG-9 enrichment at centrosomes. Since the interaction between TAC-1 L229F encoded by *tac-1(or369)* and the ZYG-9 TBR is significantly reduced in vitro (see Fig. 3), it is tempting to speculate that TAC-1 recruits ZYG-9 to centrosomes in wild-type embryos. Third, cytoplasmic levels of ZYG-9 in *tac-1(or369)* embryos are comparable to those in wild-type embryos, even though centrosomal ZYG-9 is diminished (Fig. 2D). Since these mutant embryos exhibit a canonical *zyg-9–tac-1* phenotype, we conclude that normal levels of ZYG-9 in the cytoplasm are not sufficient for correct microtubule-dependent processes. An analysis of ZYG-9 distribution in embryos, in which *tac-1* has been inactivated only partially by RNAi indicated that normal levels of ZYG-9 at centrosomes are not sufficient either (Bellanger and Gönczy, 2003). Together, these findings establish that ZYG-9 is limiting both in the cytoplasm and at centrosomes in one-cell-stage embryos. Fourth, we found that *tac-1(or455)* embryos maintained at the permissive temperature exhibit a significant diminution of TAC-1 at centrosomes and to a lesser extent in the cytoplasm (Fig. 2I), but no detectable change in ZYG-9 distribution (Fig. 2H). These embryos undergo correct microtubule-dependent processes and are fully viable (Table 1). Therefore, in contrast to ZYG-9, TAC-1 is not limiting for microtubule-dependent processes in one-cell-stage embryos. Furthermore, TAC-1 levels and distribution in *zyg-9(or628)*
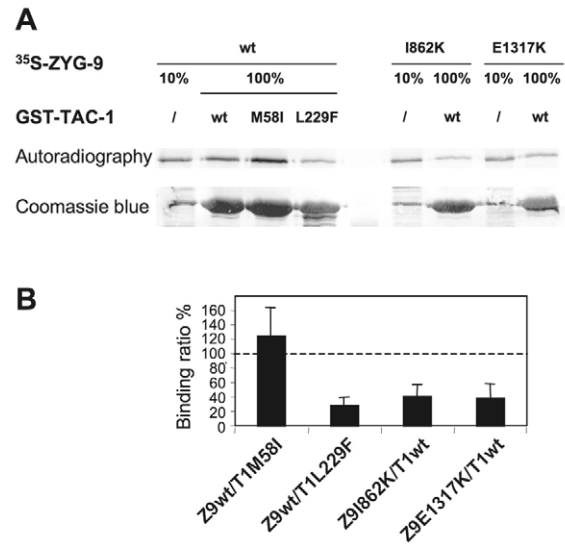

Fig. 3. Impact of select mutations on the binding between TAC-1 and ZYG-9. (A) GST pull-down experiments with wild-type, M58I or L229F GST-TAC-1 and in vitro translated [^{35}S]-labeled wild-type, I862K or E1317K ZYG-9 TBR (654-1415), as indicated. Top panels show 10% of the input material and 100% of the corresponding pulled-down material detected by autoradiography. The bottom panels show the Coomassie Blue staining of the GST-TAC-1 fusions used in each case, indicating that comparable amounts of proteins had been added. The weaker band detected in the input lanes (denoted by 10%) corresponds to a ~60-kDa protein from the in vitro transcription/translation mix. GST alone did not retain significant amounts of ZYG-9 TBR (data not shown). (B) Quantification of TAC-1–ZYG-9 binding, expressed as the percentage of each radioactive product retained on Glutathione-sepharose beads, averaged from three independent experiments, ± s.e.m. 100% corresponds to binding observed with wild-type ZYG-9 TBR and wild-type GST-TAC-1.

embryos are comparable to those in wild type (Fig. 1G), indicating that TAC-1 is not sufficient either for these processes.

ZYG-9–TAC-1 is required for anaphase spindle positioning in one-cell stage *C. elegans* embryos

We next decided to take advantage of the conditional nature of these alleles to specifically investigate the function of ZYG-9–TAC-1 during mitosis. The requirement of ZYG-9–TAC-1 during interphase has prevented an analysis of the specific requirement after this stage using RNAi or other non-conditional methods of gene inactivation. We reasoned that the new temperature-sensitive alleles might provide a means of compromising ZYG-9–TAC-1 selectively during mitosis.

Using time-lapse DIC microscopy, examination of embryos from the new mutant alleles raised at ~15°C and ~26°C indicated that short exposure to the restrictive temperature results in the canonical *zyg-9–tac-1* phenotype in the case of *zyg-9(or634)* and *tac-1(or455)* (data not shown). We used *zyg-9(or634)* to inactivate *zyg-9* function during mitosis (Fig. 4C). Animals were raised, dissected and initially observed on the microscope stage at ~15°C (Materials and Methods). Towards the end of interphase, when the two joined pronuclei moved to the cell center, the temperature was shifted to ~26°C and
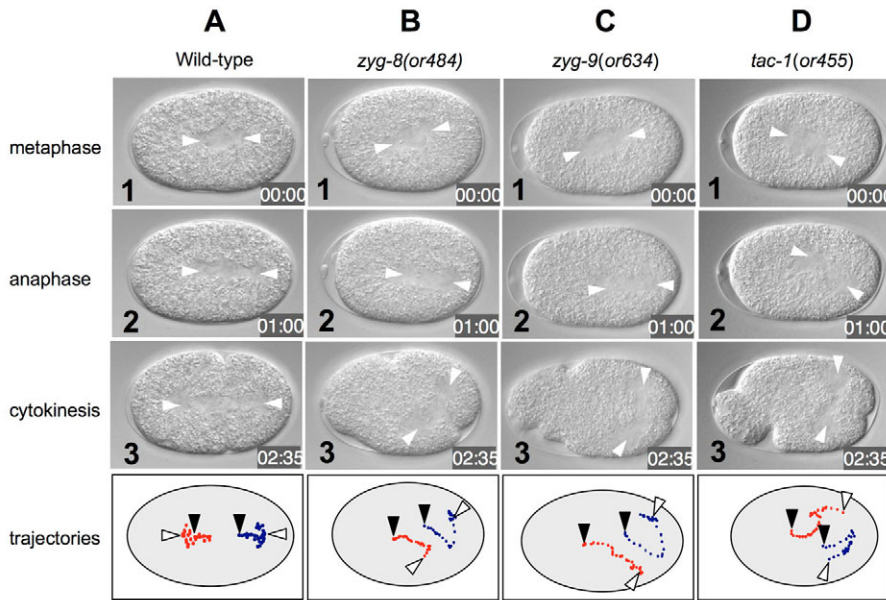
Fig. 4. *zyg-9* and *tac-1* function during mitosis to ensure correct spindle positioning. (A-D) Images from time-lapse DIC microscopy sequences of wild-type (A), *zyg-8(or484)* (B), *zyg-9(or634)* (C) or *tac-1(or455)* (D) embryos shifted to 25°C during centration/rotation; row 1, metaphase; row 2, anaphase; row 3, cytokinesis. Arrowheads point to spindle poles. Last row of panels represent the trajectories of the anterior (red) and posterior (blue) spindle poles during mitosis; spindle-pole position was plotted every 5 seconds for the entire duration of the movies; arrowheads, positions of spindle poles at the onset (black arrowheads correspond to row 1) and the end (white arrowhead correspond to row 3). Elapsed time is indicated in minutes and seconds. Embryos are ~50 μm long. Note that in the wild-type, the anterior spindle pole shifts to a sligthly posterior position before moving to a more anterior one. In 9/18 *zyg-9(or634)* and 5/23 *tac-1(or455)* embryos, spindle positioning was as depicted here, with the phenotype typically being somewhat less pronounced in *tac-1(or455)* embryos; 4/18 *zyg-9(or634)* and 13/23 *tac-1(or455)* embryos exhibited analogous but weaker spindle positioning defects, like those observed following partial RNAi-mediated inactivation of *zyg-8*; the spindle snapped in two in 3/18 *zyg-9(or634)* and 3/23 *tac-1(or455)* embryos, as is also observed in occasional *zyg-8*-mutant embryos (Gönczy et al., 2001); in 2/18 *zyg-9(or634)* and 2/23 *tac-1(or455)* embryos, spindle positioning was akin to wild type, perhaps because of incomplete or delayed inactivation. In some *zyg-9(or634)* and *tac-1(or455)* embryos, centration/rotation was incomplete (see panel D1). Anterior is left, posterior is right.

the observation continued. We found that *zyg-9(or634)* embryos treated in this manner assemble a spindle in the cell center and aligned along the anterior-posterior (A-P) axis – like in the wild type (compare Fig. 4C1 with Fig. 4A1). Strikingly, however, the spindle is displaced in an exaggerated manner towards the lateral and posterior cortex during anaphase (compare Fig. 4C2 with 4A2). These phenotypes are comparable to those observed in embryos with compromised *zyg-8* function or after nocodazole treatment during mitosis (Fig. 4B) (Gönczy et al., 2001). As shown in Fig. 4D, we observed a similar sequence of events towards the end of interphase when *tac-1(or455)* embryos were shifted to ~26°C. As anticipated from the phenotypic similarity, we found that the microtubule network in temperature-shifted *zyg-9(or634)* and *tac-1(or455)* embryos resembled that of embryos with compromised *zyg-8* function (supplementary material Fig. S3). We conclude that ZYG-9–TAC-1 is required during mitosis for correct anaphase spindle positioning in one-cell-stage *C. elegans* embryos, something that could not be tested

prior to this work due to the earlier requirements of ZYG-9–TAC-1 during the cell cycle.

ZYG-9–TAC-1 and ZYG-8 are required, in a partially redundant manner, for microtubule-dependent processes throughout the cell cycle

Our analysis indicates that ZYG-9–TAC-1 functions during mitosis, simultaneously with ZYG-8. Therefore, we set out to investigate whether these two microtubule-growth-promoting factors genetically interact during mitosis, as well as other stages of the cell cycle. To this end, we sensitized one-cell-stage embryos to the lack of growth-promoting factors throughout the cell cycle by compromising *zyg-9–tac-1* function, and addressed whether the additional inactivation of *zyg-8* results in synthetic phenotypes (Fig. 5, Table 2).

In wild-type embryos (Fig. 5A), the female pronucleus forms in the presumptive anterior. The male pronucleus, together with the two centrosomes, are in close proximity of the presumptive posterior cortex (Fig. 5A1). Thereafter, the female pronucleus moves towards the centrosomes, whereas the centrosomes and associated male pronucleus move away more slowly from the posterior cortex. After the two pronuclei have met in the posterior half of the embryo, centration and rotation of the two pronuclei and associated centrosomes ensues, which results in them moving ~20 μm away from the posterior cortex; the spindle thus sets up in the cell center and along the A-P axis (Fig. 5A2). During anaphase, the spindle elongates asymmetrically and becomes positioned slightly towards the posterior (Fig. 5A3,A5), resulting in an unequal cleavage (Fig. 5A4).

In *tac-1(RNAi)* embryos (Fig. 5B), there is sometimes more than one female pronucleus, indicative of a partially penetrant defect during the female meiotic divisions (Table 2) (Le Bot et al., 2003; Srayko et al., 2003). Apart from this, the sequence of events does not differ from that in wild type until the onset of pronuclear migration (Fig. 5B1). Thereafter, the male pronucleus and associated centrosomes move away slightly (on average 2.9 μm) from the posterior cortex, but further movement of male or female pronucleus does not occur. Moreover, centration and rotation of centrosomes and pronuclei do not take place. As a result, the spindle assembles in the cell posterior and elongates slightly, orthogonal to the A-P axis (Fig. 5B2,B3,B5). A cleavage furrow ingresses from the posterior cortex, bisecting the orthogonally placed spindle (Fig. 5B4).

The phenotype of *zyg-8(or484)*-mutant embryos (Fig. 5C) is analogous to that of null alleles of *zyg-8*, such as *zyg-8(t1650)*

A wild-type
B *tac-1(RNAi)*
C *zyg-8(or484)*
D *zyg-8(or484) tac-1(RNAi)*
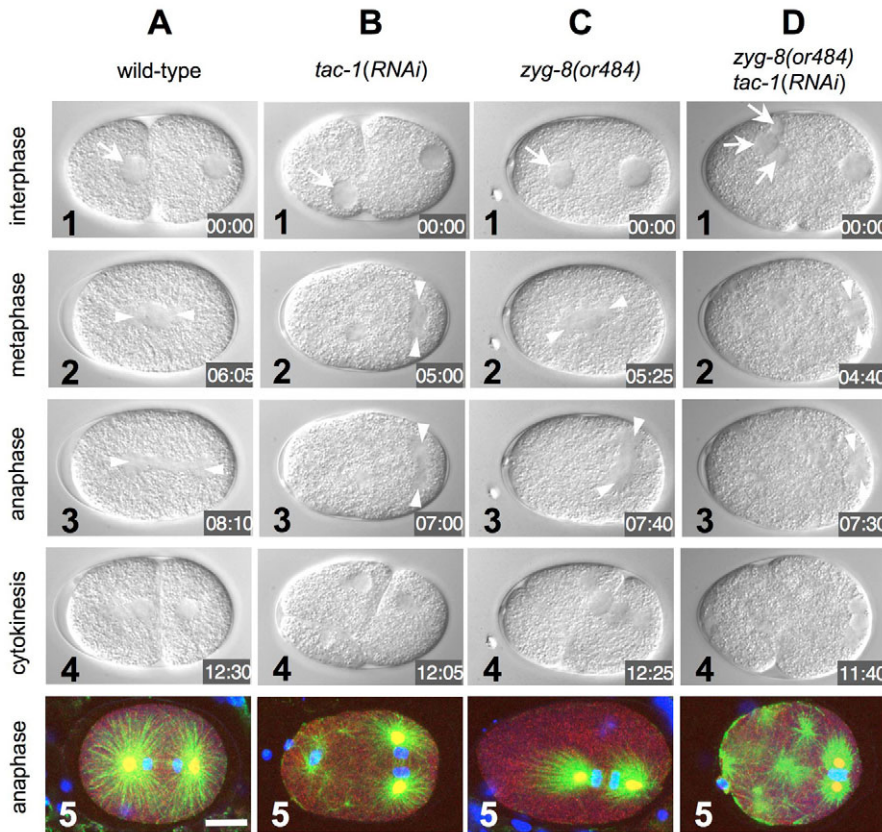
Fig. 5. Synthetic phenotypes in embryos simultaneously compromised for ZYG-9–TAC-1 and ZYG-8. (A-D) Images from time-lapse DIC microscopy sequences of wild-type (A), *tac-1(RNAi)* (B), *zyg-8(or484)* (C) and *zyg-8(or484) tac-1(RNAi)* (D) embryos; Row 1, pseudocleavage stage (interphase); row 2, metaphase; row 3, end of anaphase; row 4, cytokinesis; row 5, merged immunostainings of α-tubulin (green), SPD-5 (red) and DNA (blue), documenting the state of microtubules and centrosomes in anaphase one-cell stage embryos of these genotypes. Arrows point to female pronuclei, arrowheads to spindle poles. Elapsed time is indicated in minutes and seconds. Embryos are ~50 μm long. See Table 2 for quantifications. Note that the spindle is less elongated and less distant from the posterior cortex in *zyg-8(or484) tac-1(RNAi)* embryos (D) than in *tac-1(RNAi)* embryos (B). Note also that the cleavage furrow does not ingress to bisect the spindle in *zyg-8(or484) tac-1(RNAi)*. However, furrowing activity does take place towards the embryo anterior, orthogonal to the A-P axis, like in embryos lacking microtubules (e.g. Gönczy et al., 2001). Notice the numerous small asters present in the cytoplasm of *zyg-8(or484) tac-1(RNAi)* embryos, which might result from a larger pool of free cytoplasmic tubulin possibly promoting non-centrosomal microtubule nucleation. Anterior is left, posterior is right; bar, 10 μm.

(Gönczy et al., 2001). Apart from some embryos having more than one female pronucleus (Table 2) (Gönczy et al., 2001), the sequence of events does not differ significantly from that in wild type prior to mitosis (Fig. 5C1,C2). During anaphase, however, the spindle is displaced in an exaggerated manner towards the lateral and posterior cortex, where it often reorientates itself orthogonally to the A-P axis (Fig. 5C3,C5). Thereafter, a cleavage furrow, usually ingressing from the posterior cortex, bisects the spindle (Fig. 5C4).

Strikingly, we found that inactivating *tac-1* using RNAi in a *zyg-8(or484)* mutant results in markedly more severe cell-division defects than those observed in either *tac-1(RNAi)* embryos or *zyg-8(or484)* embryos (Fig. 5D). First, 82% of doubly compromised embryos exhibit more than one female pronucleus (Fig. 5D, left), compared with 8% in *tac-1(RNAi)* embryos and 26% in *zyg-8(or484)*-mutant embryos (Table 2). Second, the male pronucleus and associated centrosomes in doubly compromised embryos barely move away (on average 1.7 μm) from the posterior cortex during interphase (Fig. 5D1). Third, the spindle is shorter to start with and does not elongate substantially during mitosis (Fig. 5D2,D3,D5); probably, as a consequence, the cleavage furrow invariably fails to ingress in doubly compromised embryos (Fig. 5D4). Analogous synthetic phenotypes were observed by performing *tac-1(RNAi)* in a *zyg-8(t1650)* mutant or *zyg-9(RNAi)* in a *zyg-8(or484)* mutant (data not shown).

We also addressed whether increasing the levels of TAC-1 can compensate for a diminution of *zyg-8* function. Accordingly, we found that the presence of transgenic GFP-TAC-1 (Bellanger and Gönczy, 2003), in addition to that of endogenous TAC-1, improves the viability of *zyg-8(or484)*-

mutant embryos raised at a semi-permissive temperature (20.0% in *zyg-8(or484)* GFP-TAC-1, *n*=370; 8.6% in *zyg-8(or484)*, *n*=236; Materials and Methods). Overall, these findings establish that ZYG-9–TAC-1 and ZYG-8 are required, in a partially redundant manner, for microtubule-dependent

Table 2. Penetrance of phenotypic manifestations following compromising *tac-1* and/or *zyg-8* function

Embryonic genotype	Meiotic defects* (in %)	Distance from posterior cortex[†] (in μm)	Cleavage-furrow ingression[‡] (in %)
N2 (wild-type)	0 (8)	18.9 (8)	100 (8)
tac-1(RNAi)[§]	8 (25)	2.9 (21)	100 (26)
zyg-8(or484)	26[§] (29)	17.7[¶] (29)	86 (29)
tac-1(RNAi) zyg-8(or484)	82 (17)	1.7 (17)	0 (18)

Not all embryos could be analyzed for each trait. The distance from the posterior cortex in *tac-1(RNAi)* embryos (average of 2.9 μm; ±s.d.=1.1) is statistically different from that in *tac-1(RNAi) zyg-8(or484)* embryos (average of 1.7 μm; ±s.d.=1.0). Student's paired *t*-test; *P*<0.003.

*Percentage of embryos with two or more female pronuclei. A few other embryos exhibited larger polar bodies but no extra female pronucleus and were not included here.

[†]Average distance between the posterior cortex and the posterior rim of the male pronucleus at nuclear envelope breakdown (NEBD).

[‡]Percentage of embryos in which the cleavage furrow ingressed to bisect the spindle.

[§]The female pronucleus is often initially smaller than the male pronucleus in *zyg-8(or484)* mutant embryos, possibly reflecting delayed progression through the female meiotic divisions.

[¶]In 14% of *zyg-8(or484)* mutant embryos, the cleavage furrow ingressed initially before regressing in the end, probably because of the very unstable spindle positioning that preceded.

The number of embryos scored is given in parentheses.

processes during meiosis, as well as during interphase and mitosis of one-cell-stage embryos.
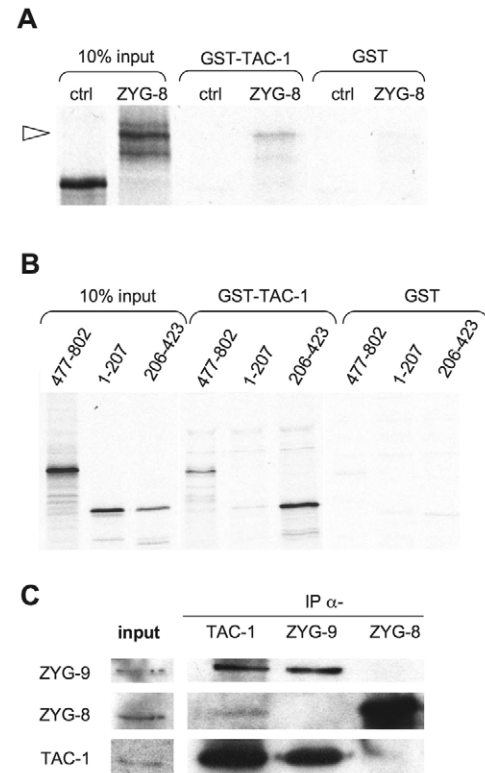
TAC-1 interacts with the doublecortin domain of ZYG-8

In an attempt to understand better the relationship between ZYG-9–TAC-1 and ZYG-8 at a molecular level, we investigated the physical interactions between these three proteins. We initially identified TAC-1 during a yeast two-hybrid screen with ZYG-8 as a bait (Bellanger and Gönczy, 2003). Previous work focused on the analysis of ZYG-9 and TAC-1 (Bellanger and Gönczy, 2003; Le Bot et al., 2003; Srayko et al., 2003), and the interaction between ZYG-8 and TAC-1 has not been investigated to date. Because TAC-1 and ZYG-9 stabilize each other, we first addressed whether the presence of TAC-1 is similarly needed for the stability of ZYG-8, and vice versa. Western-blot analysis indicates that the levels of ZYG-8 are not significantly reduced in *tac-1(RNAi)* embryonic extracts (see supplementary material Fig. S4A), nor are they reduced in the eight new *tac-1-* and *zyg-9*-mutant strains (data not shown). Reciprocally, the levels of TAC-1 are not diminished when *zyg-8* is inactivated (see supplementary material Fig. S4A). Furthermore, the subcellular distribution of ZYG-8 is not changed in *tac-1(or455)* (supplementary material Fig. S4C, compare with S4B) and that of TAC-1 is not altered in *zyg-8*-mutant embryos (supplementary material Fig. S4E, compare with S4D). Thus, in contrast to TAC-1 and ZYG-9, TAC-1 and ZYG-8 do not appear to be mutually dependent for achieving correct protein levels or subcellular distribution.

We next tested whether the interaction observed between ZYG-8 and TAC-1 by using the yeast two-hybrid assay reflects a direct association between the two proteins. As shown in Fig. 6A, we found that in vitro translated full-length ZYG-8 binds TAC-1 in a pull-down assay. Fragments of ZYG-8 that lack the doublecortin domain either fail to interact in a detectable manner (fragment 1-207) or only interact weakly (fragment 477-802) with TAC-1 (Fig. 6B). Conversely, a fragment comprising amino acids 206-423 that contains the doublecortin domain, mediates robust interaction with TAC-1 (Fig. 6B). Together, these findings indicate that the doublecortin domain of ZYG-8 is necessary and sufficient to directly interact with TAC-1. By analyzing the protein encoded by a mutant allele of *zyg-8*, we obtained evidence that the ability of the doublecortin domain of ZYG-8 to interact with TAC-1 is separate from its ability to bind microtubules. The G219E mutation in *zyg-8(or484)* alters a residue in the first β-strand of the doublecortin domain that is invariant in all proteins that share this domain (Gönczy et al., 2001; Kim et al., 2003). We found that, in contrast to wild-type ZYG-8 (see supplementary material Fig. S5A) (Gönczy et al., 2001), ZYG-8 G219E does not colocalize with microtubules in COS7 cells (see supplementary material Fig. S5B). Nevertheless, the doublecortin domain of this variant of ZYG-8 interacts with TAC-1 in yeast two-hybrid (see supplementary material Fig. S5C), indicating that association with TAC-1 does not require binding to microtubules.

TAC-1 interacts with ZYG-8 in a ZYG-9-free complex.

We next sought to address whether ZYG-8 associates with TAC-1 in vivo by performing reciprocal co-immunoprecipitation experiments using *C. elegans* embryonic

Fig. 6. ZYG-8, through its doublecortin domain, interacts with TAC-1, in a ZYG-9-free complex. (A,B) GST-pull-down experiments with (A) in vitro translated [^{35}S]-labeled full-length ZYG-8 (arrowhead) or an unrelated [^{35}S]-labeled control protein (denoted 'ctrl', see Materials and Methods), or (B) [^{35}S]-labeled ZYG-8 fragments. Shown are 10% of the input material and 100% of the material pulled-down by either GST-TAC-1 or GST. Ponceau staining indicates that comparable amounts of GST-TAC-1 and GST had been incubated with the radioactive products (data not shown). (C) Co-immunoprecipitation experiments of wild-type embryonic extracts. Extracts were immunoprecipitated with TAC-1, ZYG-8 or ZYG-9 antibodies (indicated above the lanes), and the immunoprecipitated material was analyzed by western blot using antibodies against ZYG-9, ZYG-8 or TAC-1 (indicated on the left).

extracts. As shown in Fig. 6C, we found that TAC-1 antibodies co-immunoprecipitate trace amounts of ZYG-8. By contrast, ZYG-9 antibodies do not co-immunoprecipitate detectable amounts of ZYG-8. Together, these findings indicate that, although most of TAC-1 is associated with ZYG-9 (Bellanger and Gönczy, 2003) a minor fraction of TAC-1 is associated with ZYG-8, perhaps because their interaction is restricted in time or space. Furthermore, these findings indicate that TAC-1 and ZYG-8 can form a complex in vivo that does not contain ZYG-9.

Discussion

Microtubule-dependent processes are crucial for cell division and are notably modulated by MAPs, which can act in a spatially and temporally restricted manner. In this study, we investigated in *C. elegans* embryos the contribution of the XMAP215 homologue ZYG-9 and of its associated partner

TAC-1, as well as that of the doublecortin-domain-containing MAP ZYG-8.

On the TAC-1/ZYG-9 complex

We report the identification of five new conditional alleles of ZYG-9, as well as the first three mutant alleles of TAC-1 in *C. elegans*, which also represent the first temperature-sensitive mutant alleles of a TACC protein in any organism. The positions of the mutations in these newly identified alleles underscore the importance of protein-protein interactions for correct ZYG-9 and TAC-1 function. Indeed, the seven distinct molecular lesions all target domains that mediate protein-protein interactions: in the case of *zyg-9* alleles, TOG domains or domains interacting with TAC-1 and, in the case of *tac-1* alleles, the TACC domain. That the TACC domain is mutated in the three *tac-1* alleles might not be significant, given that this domain accounts for ~80% of the entire protein. By contrast, we noticed that three out of five *zyg-9* mutations lie in the fifth HEAT repeat of TOG domains 1 or 2, a finding unlikely to be owing to chance, given that together the three HR5 regions of ZYG-9 represent only ~8% of the entire protein (see supplementary material Fig. S2). Moreover, the two other *zyg-9* mutations target residues located in domains known to interact with TAC-1 (Bellanger and Gönczy, 2003) and, indeed, cause a severe reduction in the ability to bind TAC-1 in vitro. Overall, it is tempting to speculate that TOG-domain-mediated interactions between ZYG-9 and some unidentified partner, as well as TOG-domain-independent interaction between ZYG-9 and TAC-1 play crucial roles during the first embryonic division of the nematode.

ZYG-9 and TAC-1 form a complex and are mutually dependent for its stability (Bellanger and Gönczy, 2003; Le Bot et al., 2003; Srayko et al., 2003). Therefore, prior analysis did not distinguish between ZYG-9 and TAC-1 being crucial for stimulating growth of microtubules, although the growth-promoting activity ascribed to XMAP215 family members made ZYG-9 a likely candidate. Moreover, it was not clear whether this complex acts solely at centrosomes, where it is enriched, or also in the cytoplasm. Our analysis of the new *zyg-9*- and *tac-1*-mutant alleles sheds light on these questions in several ways. First, by analyzing *zyg-9(or628)* embryos, we found that the reduction of centrosomal ZYG-9 does not result in a similar depletion of centrosomal TAC-1, raising the possibility that TAC-1 can localize to centrosomes – at the least to some extent – independently of ZYG-9. Second, by analyzing *tac-1(or369)* embryos, we found that cytoplasmic ZYG-9 is indistinguishable from the wild type. Nevertheless, *tac-1(or369)* embryos exhibit a strong phenotype, indicating that normal levels of cytoplasmic ZYG-9, by themselves, are not sufficient for function. Since normal levels of centrosomal ZYG-9 are not sufficient either (Bellanger and Gönczy, 2003), ZYG-9 levels appear to be critical both in the cytoplasm and at centrosomes to ensure correct microtubule-dependent processes in one-cell-stage embryos. Third, analyzing *tac-1(or455)* embryos at the permissive temperature, we found that a significant reduction of TAC-1 levels at centrosomes does not interfere with microtubule-dependent processes. Moreover, by analyzing *zyg-9(or628)* embryos, we found that normal levels and distribution of TAC-1 are also not sufficient for microtubule-dependent processes. Taken together, these findings establish that ZYG-9, but not TAC-1, is limiting both

in the cytoplasm and at centrosomes for promoting microtubule growth, whereas TAC-1 is important for maintaining correct ZYG-9 levels and contributing to its centrosomal enrichment.

TACC proteins appear to exert slightly distinct functions in other organisms. Thus, although the *Xenopus* TACC protein Maskin interacts with XMAP215, immunodepletion and add-back experiments in egg extracts indicate that Maskin can promote microtubule assembly without XMAP215 (O'Brien et al., 2005; Peset et al., 2005). In *Drosophila*, it has been proposed that TACC functions primarily to recruit the XMAP215 homologue Msp to centrosomes (Lee et al., 2001). TACC proteins have been implicated in tumor progression in human cells (reviewed in Raff, 2002), and it will be interesting to use the newly identified temperature-sensitive *tac-1* alleles to test whether TAC-1 is required for cell division in later stages of *C. elegans* development. Suggestively, *tac-1(or455)*-mutant animals raised at the restrictive temperature throughout development become uncoordinated (our unpublished observations), compatible with a later requirement for cell division. Therefore, the new *tac-1* alleles described in this study represent an important resource for future investigation of the role of TACC proteins during development of metazoan organisms.

On the TAC-1/ZYG-8 complex

TACC-domain-containing proteins and doublecortin-domain-containing proteins are evolutionarily conserved and we found that TAC-1 physically interacts with ZYG-8, both in vitro and in vivo. The biological significance of this physical interaction remains to be clarified. We found that ZYG-8 is not required for correct levels or distribution of TAC-1, as expected from the fact that null-alleles of *zyg-8* do not exhibit the earlier phenotypes associated with loss of *zyg-9–tac-1* function. Conversely, TAC-1 is not required for correct levels or distribution of ZYG-8, even though this could have been envisaged given that *zyg-8* mutants exhibit defects later than embryos lacking *zyg-9–tac-1*. Therefore, ZYG-8 and TAC-1 do not mutually stabilize each other, in contrast to ZYG-9 and TAC-1. Nonetheless, it remains possible that ZYG-8 somehow promotes the function of ZYG-9–TAC-1 without affecting protein levels or distribution. For instance, the kinase domain of ZYG-8 could phosphorylate ZYG-9 or TAC-1, the latter being more likely given that ZYG-8 and TAC-1 are part of a complex that does not contain ZYG-9. In this manner, ZYG-8 could modulate the activity of the ZYG-9–TAC-1 complex. There is precedent for phosphorylation modulating XMAP215 and TACC proteins. Thus, phosphorylation of XMAP215 by CDK1 dampens its growth promoting activity in vitro (Vasquez et al., 1999), whereas phosphorylation by Aurora-A activates TACC at centrosomes in *Drosophila* (Barros et al., 2005), and is similarly required for the recruitment of Maskin to the spindle poles in *Xenopus* egg extracts (Peset et al., 2005). By analogy, one could speculate that the kinase domain of ZYG-8 similarly activates TAC-1.

Together, ZYG-9–TAC-1 and ZYG-8 promote microtubule-dependent processes throughout the cell cycle

A plausible alternative to ZYG-8 modulating ZYG-9–TAC-1 activity is that the growth-promoting activities of ZYG-9–TAC-1 and that of ZYG-8, perhaps associated with TAC-1,

independently ensure efficient microtubule-dependent processes throughout the cell cycle. Compatible with this view, we found that, compromising ZYG-9–TAC-1 in addition to ZYG-8 yields more severe phenotypes than compromising either MAP alone. Doubly compromised embryos exhibit enhanced meiotic defects, more severe pronuclear migration defects during interphase, and synthetic defects in spindle elongation and cytokinesis. Therefore, ZYG-9–TAC-1 and ZYG-8 act in a partially redundant manner during meiosis, interphase and mitosis to ensure correct microtubule-dependent processes. To our knowledge, such functional redundancy between these MAPs has not, in any organism, been documented before.

Whereas ZYG-9–TAC-1 has previously been known to promote growth of microtubules early in the cell cycle (Matthews et al., 1998; Bellanger and Gönczy, 2003; Le Bot et al., 2003; Srayko et al., 2003; Srayko et al., 2005), our findings uncover that ZYG-8 functions also during interphase and not only during mitosis as previously suspected. The interphase requirement is masked by the presence of ZYG-9–TAC-1, and becomes apparent only when ZYG-9–TAC-1 and ZYG-8 are compromised simultaneously. Because anaphase in early *C. elegans* embryos is accompanied by extensive growth of astral microtubules, MAPs – such as ZYG-8 – that contribute to a lesser extent to microtubule growth throughout the cell cycle may become limiting only during anaphase. By contrast, MAPs – such as ZYG-9–TAC-1 – that contribute to a greater extent are already limiting during interphase. A combination of different MAPs contribute to the overall behavior of microtubules in other cases. For instance, a balance of the growth-promoting XMAP215 and of the microtubule-destabilizing XKCM1 determines microtubule dynamics in *Xenopus* egg extracts (Tournebize et al., 2000; Kinoshita et al., 2001). In *C. elegans* embryos, our findings establish that ZYG-9–TAC-1 and ZYG-8, two growth-promoting MAPs, ensure together the correct microtubule-dependent processes throughout the cell cycle.

Materials and Methods
Nematode strains
C. elegans strains were maintained according to standard methods (Brenner, 1974). *zyg-8*-mutant alleles have been described previously (Gönczy et al., 2001). Temperature-sensitive mutant alleles were generated in a *lin-2(e1309)* background (Encalada et al., 2000). For linkage group mapping, *tac-1(ts); him-8(e1498) IV* and *zyg-9(ts); him-8(e1498) IV* males were mated with MT3751 [*dpy-5(e61) I; rol-6(e187) II; unc-32(e189) III*], MT464 [*unc-5(e53) IV; dpy-11(e224) V; lon-2(e678) X*] hermaphrodites. All eight mutant alleles showed linkage to chromosome IV. All three *tac-1* alleles mapped to the right arm of LGII, distal to *lin-7* at map position 22.9 (*tac-1* is located at ~23.46), based on three-factor mapping with strains of the genotype *tac-1(ts)/rol-1(e91) lin-7(e1413)* II. Further mapping of *tac-1*-mutant alleles was conducted by standard three-factor crosses and SNP mapping (Brenner, 1974; Wicks et al., 2001). Sequencing of mutant alleles was performed on a pool of three independently PCR-amplified genomic DNA using the Beckman Quickstart Dye Terminator Kit and a Beckman CEQ8000 instrument, at the University of Oregon DNA Sequencing Facility.

To determine the lethality of embryos produced by homozygous *tac-1* and *zyg-9* mutants at 15°C, individual worms were allowed to lay eggs overnight followed by removal of the adults. Embryo lethality was determined 24 hours after removal of the adults by counting the number of unhatched embryos and larvae using a stereomicroscope. The same procedure was used at 26°C, except that L4 larvae raised at 15°C were shifted to the restrictive temperature of 26°C overnight, and then transferred to fresh plates and allowed to lay eggs overnight.

Unless specified otherwise, homozygous mutant animals of temperature sensitive alleles were shifted to the restrictive temperature of ~25°C for >12 hours prior to analysis for immunofluorescence or time-lapse microscopy. To compare embryonic lethality conferred by *zyg-8(or484)* to that conferred by *zyg-8(or484)* expressing GFP-TAC-1 (Bellanger and Gönczy, 2003), embryos were collected at room temperature for 7-15 hours and the population of surviving adults determined was 2 days later. For simplicity, we refer throughout the manuscript to 'mutant embryos' when mentioning the progeny derived from homozygous mutant animals.

RNAi
Bacterial strains for RNAi by feeding of *zyg-9* and of *tac-1* were generated essentially as described (Kamath et al., 2001). L4 hermaphrodites were placed onto feeding plates and incubated typically for >30 hours at 20°C before analysis. While feeding *zyg-8(or484)* animals, plates and control plates were transferred to 25°C 6-15 hours prior to analysis.

Microscopy
For most experiments, embryos were analyzed by time-lapse DIC microscopy at 23±1°C, capturing one image every 5 seconds (Gönczy et al., 1999). Movies corresponding to the embryos displayed in Figs 4 and 5 are available upon request. To ensure conditional inactivation of *tac-1* or *zyg-9* following a temperature shift, *tac-1(or455)* and *zyg-9(or634)* animals were kept at ~15°C until the time of dissection. Embryos were prepared and mounted on an agarose pad containing a thermal probe to monitor the temperature of the specimen during the experiment. The preparation was placed on the microscope stage, where the temperature was kept at 15-18°C using a custom-made fan coupled to a cooling unit. When one-cell-stage embryos were undergoing centration/rotation, the temperature was set to ~26°C, which was reached within <90 seconds.

Indirect immunofluorescence
Methanol fixation and staining of embryos for indirect immunofluorescence followed established protocols (Gönczy et al., 1999), with the following exceptions. In some cases (Fig. 2H,I), animals grown at 15°C were dissected and fixed in the cold-room to prevent heat-induced protein inactivation. Such a brief (<3 minutes) stay in the cold room did not alter the microtubule network in a significant manner in the wild type (data not shown). For analysis of mutant embryos following a brief temperature-shift (supplementary material Fig. S3), animals were placed within an Eppendorf tube into a PCR machine at 26°C for 7 minutes prior to fixation. For staining with ZYG-8 antibodies, fixation in methanol of ~1 minute was necessary to achieve robust staining of the spindle and spindle poles.

The following primary antibodies were used: 1:200 mouse anti-α-tubulin (DM1A, Sigma), 1:500 rabbit anti-TAC-1 (Bellanger and Gönczy, 2003), 1:5000 rabbit anti-ZYG-9 (Gönczy et al., 2001), 1:200 rabbit anti-ZYG-8 (Gönczy et al., 2001), 1:3000 rabbit anti-SPD-5 (Hamill et al., 2003). Secondary antibodies were 1:1000 goat anti-mouse conjugated to Alexa-Fluor-488 (Molecular Probes) and 1:1000 goat anti-rabbit conjugated to Alexa-Fluor-543. Slides were counterstained with ~1 μg/ml Hoechst-dye 33258 (Sigma) to detect DNA. Unless indicated otherwise, optical slices (~1 μm thick) were collected on an LSM510 Zeiss confocal microscope and processed using Adobe Photoshop, maintaining the relative intensities among embryos.

Quantification of ZYG-9 and TAC-1 following indirect immunofluorescence was performed on a wide-field microscope with a 63× lens using Metamorph software (Universal Imaging), analyzing 400×300 pixel images of embryos during late prometaphase (occasional embryos), during metaphase (some embryos) or anaphase (most embryos) of the first or second cell cycle, following background removal. To determine the relative levels of ZYG-9 or TAC-1 (Figs 1, 2), the average pixel intensity of the ZYG-9 or TAC-1 signal in the cytoplasm was compared with the average pixel intensity of the α-tubulin signal in two ~150-pixel circles encompassing the middle of the asters, which served as an internal control for staining efficiency. To determine the ratio between the levels of ZYG-9 or TAC-1 at centrosomes and in the cytoplasm, the average pixel intensity of the ZYG-9 or TAC-1 signal in two ~50-pixel circles centered on the centrosomes was compared with the average pixel intensity of signal in the cytoplasm. Although some pre-anaphase embryos were included to increase sample size, restricting the quantification strictly to anaphase embryos did not alter the results in a significant manner (data not shown).

Site-directed mutagenesis and GST pull-down
To generate GST-TAC-1 M58I and L229F, as well as the two ZYG-9 mutations I862K and E1317K, we mutated (site-directed mutagenesis strategy from Stratagene) pGex-TAC-1 (Bellanger et al., 2003) and a vector containing the TAC-1-binding region (TBR) of ZYG-9 (aa 654-1415) (Bellanger et al., 2003). Recombinant GST and GST-TAC-1 proteins were produced in *E. coli*, purified, dialyzed against PBS and snap-frozen. The ZYG-9 TBR, the full-length ZYG-8 or fragments thereof, as well as the first GEF domain of human Trio, were translated in vitro using the TNT T7 kit (Promega) in the presence of [^{35}S]methionine (Amersham-Pharmacia), as described (Bellanger et al., 2000). Translation efficiency was verified by SDS-PAGE and autoradiography. Of each labeled protein 1-10 μl were then incubated for 2 hours (ZYG-9) or overnight (ZYG-8) at 4°C with 5 μg of GST or GST-TAC-1 in 200 μl binding buffer (Hepes 50 mM pH 7.5, NaCl 150 mM, MgCl$_2$ 5 mM, DTT 0.1 mM and Tween-20 0.01%). The GST proteins and associated radioactive products were purified using glutathione beads, and the retained material was separated by SDS-PAGE prior to autoradiography.

Western blot and co-immunoprecipitation experiments

Western blot analysis was performed using nitrocellulose membranes (Protran, Schleicher&Schuell). Primary antibodies used were diluted in PBS with 5% milk and 0.1% Tween-20. Secondary HRP-coupled anti-mouse and anti-rabbit antibodies were diluted in PBS and used at 1:10,000. The ECL reaction was performed as recommended by the manufacturer (Amersham Pharmacia).

Co-immunoprecipitations were performed as described (Bellanger and Gönczy, 2003). Briefly, worm embryonic extract was prepared in IP buffer (Hepes 100 mM, NaCl 750 mM, MgCl$_2$ 10 mM, EDTA 50 mM, DTT 1 mM, protease inhibitors) by grinding snap-frozen embryos in a ceramic bowl. The extract was pre-cleared on proteinG-sepharose beads prior to addition of antibodies (5 μg/ml final concentration) and incubation for 2 hours at 4°C, followed by addition of proteinG-sepharose and further incubation for 1 hour at 4°C. The beads were washed once with IP buffer and twice with PBS before western blot analysis.

References

Al-Bassam, J., Larsen, N. A., Hyman, A. A. and Harrison, C. (2007). Crystal structure of a TOG domain: conserved features of XMAP215/Dis1-family TOG domains and implications for tubulin binding. *Structure* **15**, 355-362.

Andrade, M. A. and Bork, P. (1995). HEAT repeats in the Huntington's disease protein. *Nat. Genet.* **11**, 115-116.

Barros, T. P., Kinoshita, K., Hyman, A. A. and Raff, J. W. (2005). Aurora A activates D-TACC-Msps complexes exclusively at centrosomes to stabilize centrosomal microtubules. *J. Cell Biol.* **170**, 1039-1046.

Bellanger, J. M. and Gönczy, P. (2003). TAC-1 and ZYG-9 form a complex that promotes microtubule assembly in *C. elegans* embryos. *Curr. Biol.* **13**, 1488-1498.

Bellanger, J. M., Astier, C., Sardet, C., Ohta, Y., Stossel, T. P. and Debant, A. (2000). The Rac1- and RhoG-specific GEF domain of Trio targets filamin to remodel cytoskeletal actin. *Nat. Cell Biol.* **2**, 888-892.

Brenner, S. (1974). The genetics of *Caenorhabditis elegans*. *Genetics* **77**, 71-94.

Cullen, C. F. and Ohkura, H. (2001). Msps protein is localized to acentrosomal poles to ensure bipolarity of *Drosophila* meiotic spindles. *Nat. Cell Biol.* **3**, 637-642.

des Portes, V., Pinard, J. M., Billuart, P., Vinet, M. C., Koulakoff, A., Carrie, A., Gelot, A., Dupuis, E., Motte, J., Berwald-Netter, Y. et al. (1998). A novel CNS gene required for neuronal migration and involved in X-linked subcortical laminar heterotopia and lissencephaly syndrome. *Cell* **92**, 51-61.

Encalada, S. E., Martin, P. R., Phillips, J. B., Lyczak, R., Hamill, D. R., Swan, K. A. and Bowerman, B. (2000). DNA replication defects delay cell division and disrupt cell polarity in early Caenorhabditis elegans embryos. *Dev. Biol.* **228**, 225-238.

Gard, D. L. and Kirschner, M. W. (1987). A microtubule-associated protein from *Xenopus* eggs that specifically promotes assembly at the plus-end. *J. Cell Biol.* **105**, 2203-2215.

Gergely, F. (2002). Centrosomal TACCtics. *BioEssays* **24**, 915-925.

Gergely, F., Draviam, V. M. and Raff, J. W. (2003). The ch-TOG/XMAP215 protein is essential for spindle pole organization in human somatic cells. *Genes Dev.* **17**, 336-341.

Gleeson, J. G., Allen, K. M., Fox, J. W., Lamperti, E. D., Berkovic, S., Scheffer, I., Cooper, E. C., Dobyns, W. B., Minnerath, S. R., Ross, M. E. et al. (1998). Doublecortin, a brain-specific gene mutated in human X-linked lissencephaly and double cortex syndrome, encodes a putative signaling protein. *Cell* **92**, 63-72.

Gönczy, P., Schnabel, H., Kaletta, T., Amores, A. D., Hyman, T. and Schnabel, R. (1999). Dissection of cell division processes in the one cell stage *Caenorhabditis elegans* embryo by mutational analysis. *J. Cell Biol.* **144**, 927-946.

Gönczy, P., Bellanger, J. M., Kirkham, M., Pozniakowski, A., Baumer, K., Phillips, J. B. and Hyman, A. A. (2001). *zyg-8*, a gene required for spindle positioning in *C.*

elegans, encodes a doublecortin-related kinase that promotes microtubule assembly. *Dev. Cell* **1**, 363-375.

Hamill, D. R., Severson, A. F., Carter, J. C. and Bowerman, B. (2003). Centrosome maturation and mitotic spindle assembly in *C. elegans* require SPD-5, a protein with multiple coiled-coil domains. *Curr. Biol.* 13, R88-R90.

Horesh, D., Sapir, T., Francis, F., Wolf, S. G., Caspi, M., Elbaum, M., Chelly, J. and Reiner, O. (1999). Doublecortin, a stabilizer of microtubules. *Hum. Mol. Genet.* **8**, 1599-1610.

Kamath, R. S., Martinez-Campos, M., Zipperlen, P., Fraser, A. G. and Ahringer, J. (2001). Effectiveness of specific RNA-mediated interference through ingested double-stranded RNA in Caenorhabditis elegans. *Genome Biol.* **2**, RESEARCH0002.

Kemphues, K. J., Wolf, N., Wood, W. B. and Hirsh, D. (1986). Two loci required for cytoplasmic organization in early embryos of *Caenorhabditis elegans*. *Dev. Biol.* **113**, 449-460.

Kim, M. H., Cierpicki, T., Derewenda, U., Krowarsch, D., Feng, Y., Devedjiev, Y., Dauter, Z., Walsh, C. A., Otlewski, J., Bushweller, J. H. et al. (2003). The DCX-domain tandems of doublecortin and doublecortin-like kinase. *Nat. Struct. Biol.* **10**, 324-333.

Kinoshita, K., Arnal, I., Desai, A., Drechsel, D. N. and Hyman, A. A. (2001). Reconstitution of physiological microtubule dynamics using purified components. *Science* **294**, 1340-1343.

Kinoshita, K., Habermann, B. and Hyman, A. A. (2002). XMAP215: a key component of the dynamic microtubule cytoskeleton. *Trends Cell Biol.* **12**, 267-273.

Le Bot, N., Tsai, M. C., Andrews, R. K. and Ahringer, J. (2003). TAC-1, a regulator of microtubule length in the *C. elegans* embryo. *Curr. Biol.* **13**, 1499-1505.

Lee, M. J., Gergely, F., Jeffers, K., Peak-Chew, S. Y. and Raff, J. W. (2001). Msps/XMAP215 interacts with the centrosomal protein D-TACC to regulate microtubule behaviour. *Nat. Cell Biol.* **3**, 643-649.

Matthews, L. R., Carter, P., Thierry, M. D. and Kemphues, K. (1998). ZYG-9, a *Caenorhabditis elegans* protein required for microtubule organization and function, is a component of meiotic and mitotic spindle poles. *J. Cell Biol.* **141**, 1159-1168.

O'Brien, L. L., Albee, A. J., Liu, L., Tao, W., Dobrzyn, P., Lizarraga, S. B. and Wiese, C. (2005). The Xenopus TACC homologue, maskin, functions in mitotic spindle assembly. *Mol. Biol. Cell* **16**, 2836-2847.

Oegema, K. and Hyman, A. A. (2005). Cell division. In *WormBook* (ed. The *C. elegans* Research Community), doi/10.1895/wormbook.1891.1872.1891, http://www.wormbook.org.

Peset, I., Seiler, J., Sardon, T., Bejarano, L. A., Rybina, S. and Vernos, I. (2005). Function and regulation of Maskin, a TACC family protein, in microtubule growth during mitosis. *J. Cell Biol.* **170**, 1057-1066.

Raff, J. W. (2002). Centrosomes and cancer: lessons from a TACC. *Trends Cell Biol.* **12**, 222-225.

Shirasu-Hiza, M., Coughlin, P. and Mitchison, T. (2003). Identification of XMAP215 as a microtubule-destabilizing factor in *Xenopus* egg extract by biochemical purification. *J. Cell Biol.* **161**, 349-358.

Shu, T., Tseng, H. C., Sapir, T., Stern, P., Zhou, Y., Sanada, K., Fischer, A., Coquelle, F. M., Reiner, O. and Tsai, L. H. (2006). Doublecortin-like kinase controls neurogenesis by regulating mitotic spindles and M phase progression. *Neuron* **49**, 25-39.

Srayko, M., Quintin, S., Schwager, A. and Hyman, A. A. (2003). *Caenorhabditis elegans* TAC-1 and ZYG-9 form a complex that is essential for long astral and spindle microtubules. *Curr. Biol.* **13**, 1506-1511.

Srayko, M., Kaya, A., Stamford, J. and Hyman, A. A. (2005). Identification and characterization of factors required for microtubule growth and nucleation in the early *C. elegans* embryo. *Dev. Cell* **9**, 223-236.

Tournebize, R., Popov, A., Kinoshita, K., Ashford, A. J., Rybina, S., Pozniakovsky, A., Mayer, T. U., Walczak, C. E., Karsenti, E. and Hyman, A. A. (2000). Control of microtubule dynamics by the antagonistic activities of XMAP215 and XKCM1 in *Xenopus* egg extracts. *Nat. Cell Biol.* **2**, 13-19.

van Breugel, M., Drechsel, D. and Hyman, A. (2003). Stu2p, the budding yeast member of the conserved Dis1/XMAP215 family of microtubule-associated proteins is a plus end-binding microtubule destabilizer. *J. Cell Biol.* **161**, 359-369.

Vasquez, R. J., Gard, D. L. and Cassimeris, L. (1999). Phosphorylation by CDK1 regulates XMAP215 function in vitro. *Cell Motil. Cytoskeleton* **43**, 310-321.

Vidal, M. (1997). The reverse two-hybrid system. In *The Yeast Two-Hybrid System* (ed. P. Bartel and S. Fields), pp. 109-147. New York: Oxford University Press.

Wicks, S. R., Yeh, R. T., Gish, W. R., Waterston, R. H. and Plasterk, R. H. (2001). Rapid gene mapping in *Caenorhabditis elegans* using a high density polymorphism map. *Nat. Genet.* **28**, 160-164.